



**International Journal  
of  
Contemporary Advanced  
Mathematics (IJCM)**

ISSN : 2180-0030

**Volume 2, Issue 1**

Number of issues per year: 6

Copyright © 2011 Computer Science Journals. All rights reserved.

## Table of Content

**Volume 2, Issue 1, August 2011**

### **Pages**

- |         |   |
|---------|---|
| 1 - 7   | Embedding and np-Complete Problems for 3-Equitable Graphs<br><i>S. K. Vaidya, P. L. Vihol</i>                       |
| 8 – 21  | A Numerical Investigation of Breast Compression: Lesion Modeling<br><i>MacArthur L, Lorenzo M. Smith, Neal Hall</i> |
| 22 – 27 | E-Cordial Labeling of Some Mirror Graphs<br><i>S K Vaidya, N B Vyas</i>   |

# **INTERNATIONAL JOURNAL OF CONTEMPORARY ADVANCD MATHEMATICS (IJCM)**

**VOLUME 2, ISSUE 3, 2011**

**EDITED BY  
DR. NABEEL TAHIR**

ISSN (Online): 2180 - 1266

International Journal of Contemporary Advanced Mathematics (IJCM) is published both in traditional paper form and in Internet. This journal is published at the website <http://www.cscjournals.org>, maintained by Computer Science Journals (CSC Journals), Malaysia.

IJCM Journal is a part of CSC Publishers

Computer Science Journals

<http://www.cscjournals.org>

# **INTERNATIONAL JOURNAL OF COMPUTATIONAL LINGUISTICS (IJCM)**

Book: Volume 2, Issue 3, August 2011

Publishing Date: 31-08-2011

ISSN (Online): 2180-1266

This work is subjected to copyright. All rights are reserved whether the whole or part of the material is concerned, specifically the rights of translation, reprinting, re-use of illustrations, recitation, broadcasting, reproduction on microfilms or in any other way, and storage in data banks. Duplication of this publication or parts thereof is permitted only under the provision of the copyright law 1965, in its current version, and permission of use must always be obtained from CSC Publishers.

IJCM Journal is a part of CSC Publishers

<http://www.cscjournals.org>

© IJCM Journal

Published in Malaysia

Typesetting: Camera-ready by author, data conversion by CSC Publishing Services – CSC Journals, Malaysia

**CSC Publishers, 2011**

## EDITORIAL PREFACE

The International Journal of Contemporary Advanced Mathematics (IJCM) is an effective medium for interchange of high quality theoretical and applied research in Computational Linguistics from theoretical research to application development. This is the first issue of second volume of IJCM. The Journal is published bi-monthly, with papers being peer reviewed to high international standards. International Journal of Contemporary Advanced Mathematics (IJCM) publish papers that describe state of the art techniques, scientific research studies and results in computational linguistics in general but on theoretical linguistics, psycholinguistics, natural language processing, grammatical inference, machine learning and cognitive science computational models of linguistic theorizing: standard and enriched context free models, principles and parameters models, optimality theory and researchers working within the minimalist program, and other approaches.

IJCM give an opportunity to scientists, researchers, and vendors from different disciplines of Artificial Intelligence to share the ideas, identify problems, investigate relevant issues, share common interests, explore new approaches, and initiate possible collaborative research and system development. This journal is helpful for the researchers and R&D engineers, scientists all those persons who are involve in Contemporary Advanced Mathematics.

Highly professional scholars give their efforts, valuable time, expertise and motivation to IJCM as Editorial board members. All submissions are evaluated by the International Editorial Board. The International Editorial Board ensures that significant developments in image processing from around the world are reflected in the IJCM publications.

IJCM editors understand that how much it is important for authors and researchers to have their work published with a minimum delay after submission of their papers. They also strongly believe that the direct communication between the editors and authors are important for the welfare, quality and wellbeing of the Journal and its readers. Therefore, all activities from paper submission to paper publication are controlled through electronic systems that include electronic submission, editorial panel and review system that ensures rapid decision with least delays in the publication processes.

To build its international reputation, we are disseminating the publication information through Google Books, Google Scholar, Directory of Open Access Journals (DOAJ), Open J Gate, ScientificCommons, Scribd, CiteSeerX Docstoc and many more. Our International Editors are working on establishing ISI listing and a good impact factor for IJCM. We would like to remind you that the success of our journal depends directly on the number of quality articles submitted for review. Accordingly, we would like to request your participation by submitting quality manuscripts for review and encouraging your colleagues to submit quality manuscripts for review. One of the great benefits we can provide to our prospective authors is the mentoring nature of our review process. IJCM provides authors with high quality, helpful reviews that are shaped to assist authors in improving their manuscripts.

### **Editorial Board Members**

International Journal of Contemporary Advanced Mathematics (IJCM)

## **EDITORIAL BOARD**

**Editor-in-Chief (EiC)**

**Professor En-Bing Lin**

Central Michigan University (United States of America)

### **ASSOCIATE EDITORS (AEiCS)**

---

**Dr. Yang Wang**

Michigan State University

United States of America

### **EDITORIAL BOARD MEMBERS (EBMs)**

---

**Dr. Armen G. Bagdasaryan**

V.A. Trapeznikov Institute for Control Sciences

Russia

**Dr. Taher Abualrub**

American University of Sharjah

United Arab Emirates

# Embedding and Np-Complete Problems for 3-Equitable Graphs

**S. K. Vaidya**  
Department of Mathematics,  
Saurashtra University,  
RAJKOT – 360005, Gujarat(India).

samirkvaidya@yahoo.co.in

**P. L. Vihol**  
Department of Mathematics,  
Government Engineering College,  
RAJKOT – 360003, Gujarat(India).

viholprakash@yahoo.com

---

## Abstract

We present here some important results in connection with 3-equitable graphs. We prove that any graph  $G$  can be embedded as an induced subgraph of a 3-equitable graph. We have also discussed some properties which are invariant under embedding. This work rules out any possibility of obtaining any forbidden subgraph characterization for 3-equitable graphs.

**Keywords:** Embedding, NP-Complete, 3-Equitable Graph.

---

2000 Mathematics Subject Classification: 05C78

## 1. INTRODUCTION

We begin with simple, finite, connected and undirected graph  $G = (V(G), E(G))$ , where  $V(G)$  is called set of vertices and  $E(G)$  is called set of edges of a graph  $G$ . For all other terminology and notations in graph theory we follow West [1] and for number theory we follow Niven and Zuckerman [2].

**Definition 1.1** The assignment of numbers to the vertices of a graph with certain condition(s) is called graph labeling.

For detailed survey on graph labeling we refer to Gallian [3]. Vast amount of literature is available on different types of graph labeling and more than 1200 papers have been published in past four decades. As stated in Beineke and Hegde [4] graph labeling serves as a frontier between number theory and structure of graphs. Most of the graph labeling techniques trace their origin to that one introduced by Rosa [5].

### **Definition 1.2**

Let  $G = (V(G), E(G))$  be a graph with  $p$  vertices and  $q$  edges. Let  $f : V \rightarrow \{0, 1, 2, \dots, q\}$  be an injection. For each edge  $uv \in E$ , define  $f^*(uv) = |f(u) - f(v)|$ . If  $f^*(E) = \{1, 2, \dots, q\}$  then  $f$  is called  $\beta$ -valuation. Golomb [6] called such labeling as a graceful labeling and this is now the familiar term.

### **Definition 1.3**

For a mapping  $f : V(G) \rightarrow \{0, 1, 2, \dots, k-1\}$  and an edge  $e = uv$  of  $G$ , we define  $f(e) = |f(u) - f(v)|$ . The labeling  $f$  is called a  $k$ -equitable labeling if the number of vertices with the label  $i$  and the number of vertices with the label  $j$  differ by at most 1 and the number of edges with the label  $i$  and the number of edges with label  $j$  differ by at most 1. By  $v_f(i)$  we mean the number of vertices with the label  $i$  and by  $e_f(i)$  we mean the number of edges with the label  $i$ .

Thus for  $k$  - equitable labeling we must have  $|v_f(i) - v_f(j)| \leq 1$  and  $|e_f(i) - e_f(j)| \leq 1$ , where  $0 \leq i, j \leq k-1$ .

For  $k = 2$ ,  $f$  is called cordial labeling and for  $k = 3$ ,  $f$  is called 3-equitable labeling. We focus on 3-equitable labeling.

A graph  $G$  is 3-equitable if it admits a 3-equitable labeling. This concept was introduced by Cahit [7]. There are four types of problems that can be considered in this area.

- (1) How 3-equitability is affected under various graph operations.
- (2) Construct new families of 3-equitable graphs by finding suitable labeling.
- (3) Given a graph theoretic property  $P$  characterize the class of graphs with property  $P$  that are 3-equitable.
- (4) Given a graph  $G$  having the graph theoretic property  $P$ , is it possible to embed  $G$  as an induced subgraph of a 3-equitable graph  $G$ , having the property  $P$ ?

The problems of first three types are largely investigated but the problems of last type are of great importance. Such problems are extensively explored recently by Acharya et al [8] in the context of graceful graphs. We present here an affirmative answer for planar graphs, trianglefree graphs and graphs with given chromatic number in the context of 3-equitable graphs. As a consequence we deduce that deciding whether the chromatic number is less than or equal to  $k$ , where  $k \geq 3$ , is NP-complete even for 3-equitable graphs. We obtain similar result for clique number also.

## 2. Main Results

### Theorem 2.1

Any graph  $G$  can be embedded as an induced subgraph of a 3-equitable graph.

**Proof:** Let  $G$  be the graph with  $n$  vertices. Without loss of generality we assume that it is always possible to label the vertices of any graph  $G$  such that the vertex conditions for 3-equitable graphs are satisfied. i.e.  $|v_f(i) - v_f(j)| \leq 1$ ,  $0 \leq i, j \leq 2$ . Let  $V_0, V_1$  and  $V_2$  be the set of vertices with label 0, 1 and 2 respectively. Let  $E_0, E_1$  and  $E_2$  be the set of edges with label 0, 1 and 2 respectively. Let  $n(V_0), n(V_1)$  and  $n(V_2)$  be the number of elements in sets  $V_0, V_1$  and  $V_2$  respectively. Let  $n(E_0), n(E_1)$  and  $n(E_2)$  be the number of elements in sets  $E_0, E_1$  and  $E_2$  respectively.

**Case 1:**  $n \equiv 0 \pmod{3}$

**Subcase 1:**  $n(E_0) \neq n(E_1) \neq n(E_2)$ .

Suppose  $n(E_0) < n(E_1) < n(E_2)$ . Let  $|n(E_2) - n(E_0)| = r > 1$  and  $|n(E_2) - n(E_1)| = s > 1$ . The new graph  $H$  can be obtained by adding  $r + s$  vertices to the graph  $G$ .

Define  $r + s = p$  and consider a partition of  $p$  as  $p = a + b + c$  with  $|a - b| \leq 1, |b - c| \leq 1$  and  $|c - a| \leq 1$ .

Now out of new  $p$  vertices label  $a$  vertices with 0,  $b$  vertices with 1 and  $c$  vertices with 2. i.e. label the vertices  $u_1, u_2, \dots, u_a$  with 0,  $v_1, v_2, \dots, v_b$  with 1 and  $w_1, w_2, \dots, w_c$  with 2. Now we adapt the following procedure.

**Step 1:** To obtain required number of edges with label 1.

- Join  $s$  number of elements  $v_i$  to the arbitrary element of  $V_0$ .
- If  $b < s$  then join  $(s - b)$  number of elements  $u_1, u_2, \dots, u_{s-b}$  to the arbitrary element of  $V_1$ .
- If  $a < s - b$  then join  $(s - a - b)$  number of vertices  $w_1, w_2, \dots, w_{s-b-a}$  to the arbitrary element of  $V_1$ .

Above construction will give rise to required number of edges with label 1.

**Step 2:** To obtain required number of edges with label 0.

- Join remaining number of  $u_i$ 's (which are left at the end of step 1) to the arbitrary element of  $V_0$ .

- Join the remaining number of  $v_i$ 's(which are left at the end of step 1) to the arbitrary element of  $V_1$ .
- Join the remaining number of  $w_i$ 's(which are left at the end of step 1) to the arbitrary element of  $V_2$ .

As a result of above procedure we have the following vertex conditions and edge conditions.

$$|v_f(0) - v_f(1)| = |n(V_0) + a - n(V_1) - b| \leq 1,$$

$$|v_f(1) - v_f(2)| = |n(V_1) + b - n(V_2) - c| \leq 1,$$

$$|v_f(2) - v_f(0)| = |n(V_2) + c - n(V_0) - a| \leq 1$$

and

$$|e_f(0) - e_f(1)| = |n(E_0) + n(E_2) - n(E_0) - n(E_1) - n(E_2) + n(E_1)| = 0,$$

$$|e_f(1) - e_f(2)| = |n(E_1) + n(E_2) - n(E_1) - n(E_2)| = 0,$$

$$|e_f(2) - e_f(0)| = |n(E_2) - n(E_0) - n(E_2) + n(E_0)| = 0.$$

Similarly one can handle the following cases.

$$n(E_0) < n(E_2) < n(E_1),$$

$$n(E_2) < n(E_0) < n(E_1),$$

$$n(E_1) < n(E_2) < n(E_0),$$

$$n(E_2) < n(E_1) < n(E_0),$$

$$n(E_1) < n(E_0) < n(E_2).$$

**Subcase 2:**  $n(E_i) = n(E_j) < n(E_k), i \neq j \neq k, 0 \leq i, j, k \leq 2$

Suppose  $n(E_0) = n(E_1) < n(E_2)$

$$|n(E_2) - n(E_0)| = r$$

$$|n(E_2) - n(E_1)| = r$$

The new graph  $H$  can be obtained by adding  $2r$  vertices to the graph  $G$ .

Define  $2r = p$  and consider a partition of  $p$  as  $p = a + b + c$  with  $|a - b| \leq 1, |b - c| \leq 1$  and  $|c - a| \leq 1$ .

Now out of new  $p$  vertices, label  $a$  vertices with 0,  $b$  vertices with 1 and  $c$  vertices with 2. i.e. label the vertices  $u_1, u_2, \dots, u_a$  with 0,  $v_1, v_2, \dots, v_b$  with 1 and  $w_1, w_2, \dots, w_c$  with 2. Now we adapt the following procedure.

### **Step 1:**

To obtain required number of edges with label 0.

- Join  $r$  number of elements  $u_i$ 's to the arbitrary element of  $V_0$ .
- If  $a < r$  then join  $(r - a)$  number of elements  $v_1, v_2, \dots, v_{r-a}$  to the arbitrary element of  $V_1$ .
- If  $b < r - a$  then join  $(r - a - b)$  number of vertices  $w_1, w_2, \dots, w_{r-a-b}$  to the arbitrary element of  $V_2$ .

Above construction will give rise to required number of edges with label 0.

### **Step 2:**

To obtain required number of edges with label 1.

- Join remaining number of  $w_i$ 's (which are not used at the end of step 1) to the arbitrary element of  $V_1$ .
- Join the remaining number of  $v_i$ 's (which are not used at the end of step 1) to the arbitrary element of  $V_0$ .
- Join the remaining number of  $u_i$ 's (which are not used at the end of step 1) to the arbitrary element

of  $V_1$ .

Similarly we can handle the following possibilities.

$$n(E_1) = n(E_2) < n(E_0)$$

$$n(E_0) = n(E_2) < n(E_1)$$

**Subcase 3:**  $n(E_i) < n(E_j) = n(E_k), i \neq j \neq k, 0 \leq i, j, k \leq 2$

Suppose  $n(E_2) < n(E_0) = n(E_1)$

Define  $|n(E_2) - n(E_0)| = r$

The new graph  $H$  can be obtained by adding  $r$  vertices to the graph  $G$  as follows .

Consider a partition of  $r$  as  $r = a + b + c$  with  $|a - b| \leq 1, |b - c| \leq 1$  and  $|c - a| \leq 1$ .

Now out of new  $r$  vertices label  $a$  vertices with 0,  $b$  vertices with 1 and  $c$  vertices with 2 .i.e. label the vertices  $u_1, u_2, \dots, u_a$  with 0,  $v_1, v_2, \dots, v_b$  with 1 and  $w_1, w_2, \dots, w_c$  with 2 . Now we adapt the following procedure.

**Step 1:**

To obtain required number of edges with label 2.

- Join  $r$  number of vertices  $w_i$ 's to the arbitrary element of  $V_0$ .
- If  $c < r$  then join  $r - c$  number of elements  $u_1, u_2, \dots, u_{r-c}$  to the arbitrary element of  $V_2$ .

Above construction will give rise to required number of edges with label 2 .

At the end of this step if the required number of 2 as edge labels are generated then we have done. If not then move to step 2 . This procedure should be followed in all the situations described earlier when  $n(E_2) < n(E_0)$  or  $n(E_2) < n(E_1)$  .

**Step 2:**

To obtain the remaining (at the end of step 1) number of edges with label 2 .

- If  $k$  number of edges are required after joining all the vertices with label 0 and 2 then add  $k$  number of vertices labeled with 0,  $k$  number of vertices labeled with 1 and  $k$  number of vertices labeled with 2 . Then vertex conditions are satisfied.
- Now we have  $k$  number of new vertices with label 2,  $k$  number of new vertices with label 0 and  $2k$  number of new vertices with label 1.
- Join  $k$  new vertices with label 2 to the arbitrary element of the set  $V_0$ .
- Join  $k$  new vertices with label 0 to the arbitrary element of the set  $V_2$ .
- Join  $k$  new vertices with label 1 to the arbitrary element of set  $V_0$ .
- Join  $k$  new vertices with label 1 to the arbitrary element of the set  $V_1$ .

**Case 2:**  $n \equiv 1(mod 3)$  .

**Subcase 1:**  $n(E_i) \neq n(E_j) \neq n(E_k), i \neq j \neq k, 0 \leq i, j, k \leq 2$  .

Suppose  $n(E_0) < n(E_1) < n(E_2)$  Let  $|n(E_2) - n(E_0)| = r > 1$  and  $|n(E_2) - n(E_1)| = s > 1$  .

Define  $r + s = p$  and consider a partition of  $p$  such that  $p = a + b + c$  with

$$|n(V_0) + a - n(V_1) - b| \leq 1$$

$$|n(V_1) + b - n(V_2) - c| \leq 1$$

$$|n(V_0) + a - n(V_2) - c| \leq 1 .$$

Now we can follow the procedure which we have discussed in case-1.

**Case 3:**  $n \equiv 2(mod 3)$

We can proceed as case-1 and case-2.

Thus in all the possibilities the graph  $H$  resulted due to above construction satisfies the conditions for 3-equitable graph. That is, any graph  $G$  can be embedded as an induced subgraph of a 3-

equitable graph.

For the better understanding of result derived above consider following illustrations.

**Illustration 2.2**

For a Graph  $G = C_9$  we have  $n(E_0) = 0$ ,  $n(E_1) = 6$ ,  $n(E_2) = 3$ .

Now  $|n(E_1) - n(E_0)| = 6 = r$ ,  $|n(E_1) - n(E_2)| = 3 = s$ .

This is the case related to subcase (1) of case (1).

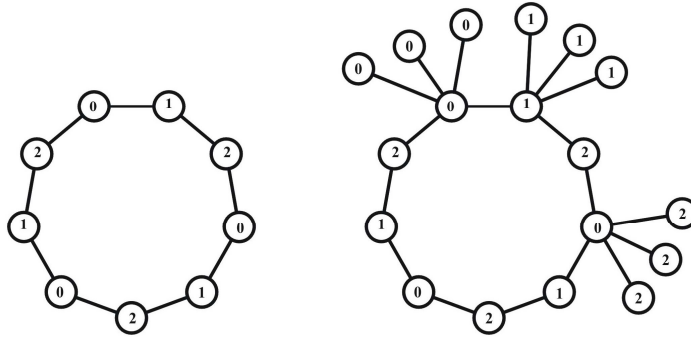


**FIGURE 1:**  $C_9$  and its 3-equitable embedding

**Procedure to construct  $H$  :**

**Step 1:**

- Add  $p = r + s = 6 + 3 = 9$  vertices in  $G$  and partition  $p$  as  $p = a + b + c = 3 + 3 + 3$ .
- Label 3 vertices with 0 as  $a = 3$ .
- Label 3 vertices with 1 as  $b = 3$ .
- Label 3 vertices with 2 as  $c = 3$ .

**Step 2:**

- Join the vertices with 0 and 1 to the arbitrary element of the set  $V_0$  and  $V_1$  respectively.
- Join the vertices with label 2 to the arbitrary element of set  $V_0$ .

The resultant graph  $H$  is shown in Figure 1 is 3-equitable.

**Illustration 2.3**

Consider a Graph  $G = K_4$  as shown in following Figure 2 for which  $n(E_0) = 1$ ,  $n(E_1) = 4$ ,  $n(E_2) = 1$ .

Here  $|n(E_1) - n(E_0)| = 3 = r$ ,  $|n(E_1) - n(E_2)| = 3 = s$  i.e.  $r = s$ .

This is the case related to subcase (2) of case (2).

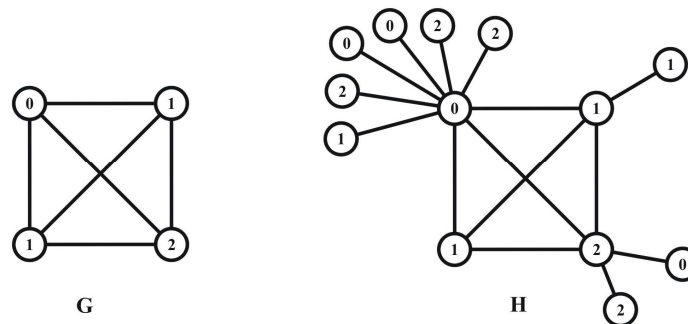


**FIGURE 2:**  $K_4$  and its 3-equitable embedding

**Procedure to construct  $H$  :**

**Step 1:**

- Add  $p = 2r = 3 + 3 = 6$  vertices in  $G$  and partition  $p$  as  $p = a + b + c = 2 + 1 + 3$ .
- Label 2 vertices with 0 as  $a = 2$ .
- Label 1 vertex with 1 as  $b = 1$ .
- Label 3 vertices with 2 as  $c = 2$ .

**Step 2:**

- Join the vertices with label 0 to the arbitrary element of the set  $V_0$  and join one vertex with label 2 to the arbitrary element of  $V_2$ .
- join the remaining vertices with label 2 with the arbitrary element of set  $V_0$ .

**Step 3:**

- Now add three more vertices and label them as 0, 1 and 2 respectively.
- Now join the vertices with label 0 and 2 with the arbitrary elements of  $V_2$  and  $V_0$  respectively.
- Now out of the remaining two vertices with label 1 join one vertex with arbitrary element of set  $V_0$  and the other with the arbitrary element of set  $V_1$ .

The resultant graph  $H$  shown in Figure 2 is 3-equitable.

**Corollary 2.4** Any planar graph  $G$  can be embedded as an induced subgraph of a planar 3-equitable graph.

**Proof:** If  $G$  is planar graph. Then the graph  $H$  obtained by Theorem 2.1 is a planar graph.

**Corollary 2.5** Any triangle-free graph  $G$  can be embedded as an induced subgraph of a triangle free 3-equitable graph.

**Proof:** If  $G$  is triangle-free graph. Then the graph  $H$  obtained by Theorem 2.1 is a triangle-free graph.

**Corollary 2.6** The problem of deciding whether the chromatic number  $\chi \leq k$ , where  $k \geq 3$  is NP-complete even for 3-equitable graphs.

**Proof:** Let  $G$  be a graph with chromatic number  $\chi(G) \geq 3$ . Let  $H$  be the 3-equitable graph constructed in Theorem 2.1, which contains  $G$  as an induced subgraph. Since  $H$  is constructed by adding only pendant vertices to  $G$ . We have  $\chi(H) = \chi(G)$ . Since the problem of deciding whether the chromatic number  $\chi \leq k$ , where  $k \geq 3$  is NP-complete [9]. It follows that deciding whether the chromatic number  $\chi \leq k$ , where  $k \geq 3$ , is NP-complete even for 3-equitable graphs.

**Corollary 2.7** The problem of deciding whether the clique number  $\omega(G) \geq k$  is NP-complete even when restricted to 3-equitable graphs.

**Proof:** Since the problem of deciding whether the clique number of a graph  $\omega(G) \geq k$  is NP-complete [9] and  $\omega(H) = \omega(G)$  for the 3-equitable graph  $H$  constructed in Theorem 2.1, the above result follows.

**3. Concluding Remarks**

In this paper, we have considered the general problem. Given a graph theoretic property  $P$  and a graph  $G$  having  $P$ , is it possible to embed  $G$  as an induced subgraph of a 3-equitable graph  $H$  having the property  $P$ ? As a consequence we derive that deciding whether the chromatic number  $\chi \leq k$ , where  $k \geq 3$ , is NP-complete even for 3-equitable graphs. We obtain similar result for clique number. Moreover this work rules out any possibility of forbidden subgraph characterization for 3-equitable graph. Analogous work for other graph theoretic parameters like domination number, total domination number, fractional domination number etc. and graphs admitting various other types of labeling can be carried out for further research.

## REFERENCES

- [1] D B West. Introduction To Graph Theory, Prentice-Hall of India, 2001
- [2] I Niven and H Zuckerman. An Introduction to the Theory of numbers, Wiley Eastern, New Delhi, 1972.
- [3] J A Gallian. A dynamic survey of graph labeling, The Electronics Journal of Combinatorics, 17, #DS6, 2010.
- [4] L W Beineke and S M Hegde. "Strongly Multiplicative Graphs", Discuss.Math.Graph Theory, 21, pp. 63-75, 2001.
- [5] A Rosa. "On Certain Valuation of the Vertices of a Graph", Theory of Graphs (Internat. Symposium, Rome, July 1966) Gordon and Breach, N.Y. and Dunod Paris, pp. 349-355, 1967.
- [6] S W Golomb. "How to Number a Graph" in: Graph Theory and Computing, R.C.Read, (Eds.), Academic Press, New York, pp. 23-37, 1972.
- [7] I Cahit. "On Cordial and 3-equitable Labeling of Graphs",Utilitas.Math, 37, pp. 189-198, 1990.
- [8] B D Acharya, S B Rao, S Arumugam, "Embeddings and NP-Complete problems for Graceful Graphs" in: B D Acharya, S Arumugam, A Rosa (Eds.),Labeling of Discrete Structures and Applications, Narosa Publishing House, New Delhi, pp. 57-62, 2008.
- [9] M R Garey and D S Johnson. Computers and Intractability- A guide to the theory of NP-Completeness, W.H.Freeman and Company, 1979.

# A Numerical Investigation of Breast Compression: Lesion Modeling

## MacArthur L

*Stewart/Department of Mechanical Engineering  
Rochester, MI 48309, USA*

*mlstewar@oakland.edu Oakland University*

## Lorenzo M. Smith

*/ Department of Mechanical Engineering  
Oakland University  
Rochester, MI 48309, USA*

*L8smith@oakland.edu*

## Neal Hall

*Department of Radiology  
St. Joseph Mercy Hospital  
Pontiac, MI 48341, USA*

*NealHall@rossmed.edu*

---

### Abstract

Researchers have developed finite element (FE) models from preoperative medical images to simulate intraoperative breast compression. Applications for these FE models include mammography, non-rigid image registration, and MRI guided biopsy. Efficient FE breast models have been constructed that model suspect lesions as a single element or node within the FE breast mesh. At the expense of efficiency, other researchers have modeled the actual lesion geometry within the FE breast mesh (conformal breast-lesion mesh). Modeling the actual lesion geometry provides lesion boundary spatial information, which is lost in FE breast models that model suspect lesions as a single element or node within the FE breast mesh.

In this paper, we used a commercial finite element analysis (FEA) program to construct a biomechanical breast model from patient specific MR volumes. A laterally situated lesion was identified in the diagnostic MRI. We used the FE model to simulate breast compression during an MRI guided biopsy. Our objective was to investigate the efficacy of independently discretizing the breast and lesion geometries and using a kinematic constraint to associate the lesion nodes to the nodes in the breast mesh based on their isoparametric position.

This study showed that it is possible to construct an accurate and efficient FE breast model that considers the actual lesion geometry. With 61 mm of breast compression, the lesion centroid was localized to within 3.8 mm of its actual position. As compared to a conformal breast-lesion FE mesh, the element count was also reduced by 53%.

These findings suggest that it is possible to predict the position of a suspect lesion's centroid and boundary within clinical time constraints (< 30 minutes).

**Keywords:** Breast, Finite Element Analysis, Breast Compression, lesions, MRI Guided Biopsy.

---

## 1. INTRODUCTION

An MRI guided biopsy requires the radiologist to localize the suspect lesion with the breast compressed between rigid plates. However, the suspect lesion is generally identified from a diagnostic MRI exam with breast freely hanging under the force of gravity. There are several potential challenges associated with localizing a suspect breast lesion including patient positioning, visibility of the lesion may fade after contrast injection, menstrual cycles, and lesion deformation. Researchers have constructed FE models that simulate breast compression with the intent of minimizing these challenges [1]. Other applications for these FE breast models included mammography [2], and non-rigid medical image registration [3], [4], [5]. For the researchers selected in this study, three FE lesion modeling methods were considered: 1) the suspect lesion was modeled as an element within the breast mesh, 2) researchers modeled suspect

lesions as point or node within the FE breast mesh, and 3) the actual geometry of the suspect lesion was modeled within the FE breast mesh, conformal breast-lesion mesh.

First, Azar et al. [1] constructed a FE breast model from MRI data of a healthy volunteer using an all hexahedral mesh. The breast contained a cyst, and it was modeled as a single element within the FE breast mesh. These researchers proposed discretizing the breast geometry with an average element size equal to the size of the suspect lesion. The error between the actual and predicted cyst position was (4.4, 1.9, 1.3), in mm.

Second, Zhang et al. [5] constructed a FE breast model from patient specific MRI data using an all tetrahedral mesh, 2<sup>nd</sup> order tetrahedral. A suspect feature was identified in corresponding mammography images. They modeled the suspect feature by tracking a point in the FE breast model. A suspect lesion was identified in the CC (cranio-caudal) view, and projected to the corresponding compressed FE model. The FE model was decompressed followed by compressing it into the MLO (mediolateral oblique) direction. The predicted position of the suspect lesion was within 2.3 mm of its actual position in the MLO view.

Third, the actual geometry of the suspect lesion was modeled within the solid breast mesh. Maintaining nodal connectivity, the lesion geometry was captured into the breast solid mesh by increasing the mesh density in the vicinity of the lesion and manipulating the position of these nodes to match the lesion's surface profile [3]. This FE modeling method was used to develop a non-rigid image registration validation procedure.

There are pros and cons associated with these lesion modeling methods. Discretizing the breast geometry and differentiating suspect lesions by assigning lesion material properties to elements in the vicinity of the actual lesion is computationally efficient; the average element edge length is a function of only the breast geometry's length scale. However, the lesion's length scale is much smaller. The lesion's centroid may be accurately predicted, but the details regarding the boundary of the lesion are lost. In contrast modeling the actual geometry, conformal breast-lesion mesh, eliminates the shortfalls stated above, but it is more computationally expensive. The overall size of the FE breast mesh depends on both the breast and lesion length scales.

The objective of this paper was to investigate the efficacy of independently discretizing the breast and lesion geometries and using a kinematic constraint to associate the lesion nodes to the nodes in the breast mesh based on their isoparametric position. We developed a patient specific biomechanical FE breast model from a diagnostic breast MR volume and the corresponding localizing MR volume from an MRI guided biopsy. The model was used to simulate the associated intraoperative breast compression. The following assumptions were considered in this study:

- Fat and fibroglandular tissues are the primary contributors to the kinematic behavior of the female breast [6]
- Breast tissue is homogeneous, isotropic, nonlinear, and nearly incompressible [7], [8]
- The Neo-Hookean material model adequately models the constitutive relationships of breast tissue [2], [4]
- The breast was allowed to freely hang during the diagnostic MRI
- Prior to compressing the breast in preparation for the biopsy, the breast was allowed to freely hang
- The sternum is stable and reproducible
- The breast coupled with the rigid plates form a conservative system
- For clinical use, predicted results should be available within 30 minutes [1]

Our FEA methodology was verified by visual inspection of the deformed surface profile, calculating the difference between the simulated and actual lesion travel, and overlaying the actual lesion onto the numerical results.

The major contributions to the published literature from this study include:

- Ability to independently discretize the breast geometry and the actual lesion geometry
- Ability to replicate surface boundary conditions including the compression and immobilization plates, and the introducer sheath (biopsy equipment)
- A FE breast model verification method that uses only the breast diagnostic and biopsy MR volumes

## 2. FINITE ELEMENT METHOD AND ELASTICITY FOR MODELING BREAST TISSUE

Constructing a FE model of the female breast requires the analyst to consider nonlinear characteristics. Since the intraoperative breast compression was finite, 61 mm, and the breast tissue material behavior was assumed hyperelastic, nonlinear geometry and nonlinear material theory was considered in this investigation. An overview of nonlinear geometry and nonlinear material theory, applicable to this research, is presented in this section. This section begins with a brief discussion on the linear tetrahedral Herrmann formulated FE element which was used to discretize the computational domain.

### 2.1 GOVERNING FUNCTIONAL

Finite elements that are formulated based on linear elastic theory are not valid for Poisson's ratio ( $\nu$ ) approaching 0.5 due to volumetric locking. Volumetric or element locking is a condition that occurs when the element is unable to distort while simultaneously meeting the incompressibility constraint [9]. The numerical solution of these equations may result in large errors due the corresponding kinematic constraints on the admissible displacement fields.

Herrmann formulated finite elements overcome this limitation for incompressible and nearly incompressible materials. In addition to nodal displacement, hydrostatic pressure is an independent variable in the element formulation.

In this research, the FE breast mesh was discretized using the linear tetrahedral Herrmann formulated finite element. This is a 5 node isoparametric element with an additional pressure degree of freedom at each of the four corner nodes [10], Fig. (1). The shape function for the center node is a bubble function. For this reason, the displacements and the coordinates for the element are linearly distributed along the element boundaries. The stiffness of this element is formed using four Gaussian integration points. The degrees of freedom of the center node are condensed out of the element before being assembled in the global matrix [10]. Because of this, it does not add to the computational expense of the FE model.

This element was formulated from the perturbed Lagrangian variational principle,

$$\int_V \left[ W_{dev.} + W_{vol.} - \frac{P^2}{2K} \right] dV - \int_S f_i u_i dS, \quad (1)$$

which is based on the on Herrmann variational theorem [11] [12]. In equation (1), the variables  $W_{dev.}$ ,  $W_{vol.}$ ,  $P$ ,  $K$ ,  $f_i$ , and  $u_i$  are the deviatoric strain energy density, volumetric strain energy density, hydrostatic pressure, bulk modulus, nodal load vector, and nodal displacement vector, respectively. Herrmann's variational theorem,

$$\int_V G \left[ I_1^2 - 2I_2 + 2\nu P I_1 - \nu(1-2\nu) P^2 \right] dV - \int_S f_i u_i dS, \quad (2)$$

and the corresponding differential equation are applicable over the entire range of admissible Poisson's ratios,  $0 \leq \nu \leq 0.5$ . The symbols  $G$ ,  $I_1$ , and  $I_2$  are the shear modulus of elasticity, 1st strain invariant, and 2nd strain invariant, respectively. This functional and the corresponding governing differential equation both describe the same physical problem. The governing differential equation can be derived by considering Euler equations [13], [14]. Equation (2) and its Euler equation counterpart are typically called the weak and strong forms of the governing equation, respectively.

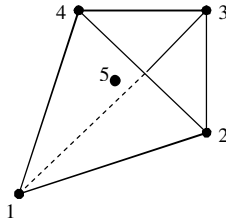


FIGURE 1: 1 Linear tetrahedral Herrmann formulated element

### 2.2 Nonlinear Geometry

An MRI guided breast biopsy results in finite breast deformation which means that geometric changes between the undeformed and compressed breast are not negligible. When finite deformations are present, geometric non-linearity should be considered for accurate FE modeling. Geometric non-linearity is usually resolved by writing the equilibrium equations in incremental form  $[K]\{\Delta D\} = \{\Delta R\}$ . In this mathematical relationship  $[K]$ ,  $\{D\}$ , and  $\{R\}$  are the stiffness matrix, element displacement vector, and nodal load vector, respectively. The  $[K]$  is a function of  $\{D\}$  which is computed iteratively. Iterating continues until the magnitude of the residual force vector is smaller than the specified tolerance. The residual force vector is defined by the difference between the external and internal force vectors. Once the convergence tolerance is satisfied, the current  $\{D\}$  becomes the sum of the preceding  $\{\Delta D\}$ 's, and the current  $[K]$  is used to calculate the next displacement increment. The displacement vector and stiffness matrix are updated and the process is repeated until the specified external loading condition is applied. Simply stated, the load-displacement curve is approximated as a series of line segments [13].

In this research, large displacement-large strain theory is assumed. Breast tissue displacements were analyzed in Lagrangian coordinates. The displacement, differentiation, and integration are referenced back to the original domain in the Lagrangian approach. As the displacement increases higher order terms are added to the strain-displacement relationship in order to account for geometric non-linearity. Lagrangian coordinates are typically used where large strains are present [15].

### 2.3 Material Non-linearity

The breast tissue constitutive relationships were modeled using the Neo-Hookean hyperelastic material model. The stress-strain relationship for a hyperelastic material is defined by a strain energy density function,

$$S_i = \frac{\partial W}{\partial \lambda_i}, \tag{3}$$

where  $S_i$ ,  $W$ , and  $\lambda_i$  are the second Piola-Kirchoff stress, strain energy density, and principle stretches, respectively [15]. Depending on the type of hyperelastic model, the strain energy function is written as a function of strain invariants or stretch ratios, defined in by:

$$\begin{aligned} I_1 &= \lambda_1^2 + \lambda_2^2 + \lambda_3^2 \\ I_2 &= \lambda_1^2 \lambda_2^2 + \lambda_2^2 \lambda_3^2 + \lambda_3^2 \lambda_1^2 \\ I_3 &= \lambda_1^2 \lambda_2^2 \lambda_3^2. \end{aligned} \tag{4}$$

The terms in equation (4) are derived from the deformation gradient,  $F_{ij}$ . The deformation gradient maps position vectors in the reference (undeformed) configuration,  $X_i$ , to the corresponding location in the deformed geometry,  $x_i$  [9],

$$\tag{5}$$

$$F_{ij} = \frac{\partial x_i}{\partial X_j}; \quad i, j = 1, 2, 3.$$

The finite deformation formulation defines the current position of a point,  $x_i$ , by adding the displacement,  $u_i$ , to the corresponding reference (undeformed) position of the point,  $X_i$  [9],

$$x_i = X_i + u_i. \quad (6)$$

The Neo-Hookean ( $W^{NH}$ ) material model assumes that the strain energy density, elastically stored energy per unit volume, is a polynomial function of the principle strain invariants. This strain energy density function contains only the first order strain invariant term [11],

$$W^{NH} = C_{10}(I_1 - 3). \quad (7)$$

The variable  $C_{10}$  is the material parameter which is derived from curve fitting the stress-strain data. Equation (7) is derived by expanding  $I_1$ , equation (4), into a power series and neglecting higher order terms [15], deviatoric component.

### 3.0 MRI Derived Finite Element Breast Model

Three commercial computer programs were used as our primary research tools. 1) ANALYZE [16] was used to view and manipulate the MR images. ANALYZE is a biomedical image viewing software developed by the Mayo Clinic. 2) The computational domain was discretized using HyperMesh [17]. HyperMesh is a FEA pre-processor, Altair Engineering, Inc. 3) Except for meshing, our FEA model was constructed and processed using MARC/Mentat which is a multi-purpose nonlinear FEA software package, MSC Software Corporation.

Figure 2 gives a general overview on how we constructed our FE model. This section is arranged into 6 subsections that discuss the components of our FE model which include: 1) MRI data and geometry construction, 2) rigid registration, 3) geometry discretization, 4) material properties and material model selection, 5) boundary conditions, and 6) numerical solution methods.

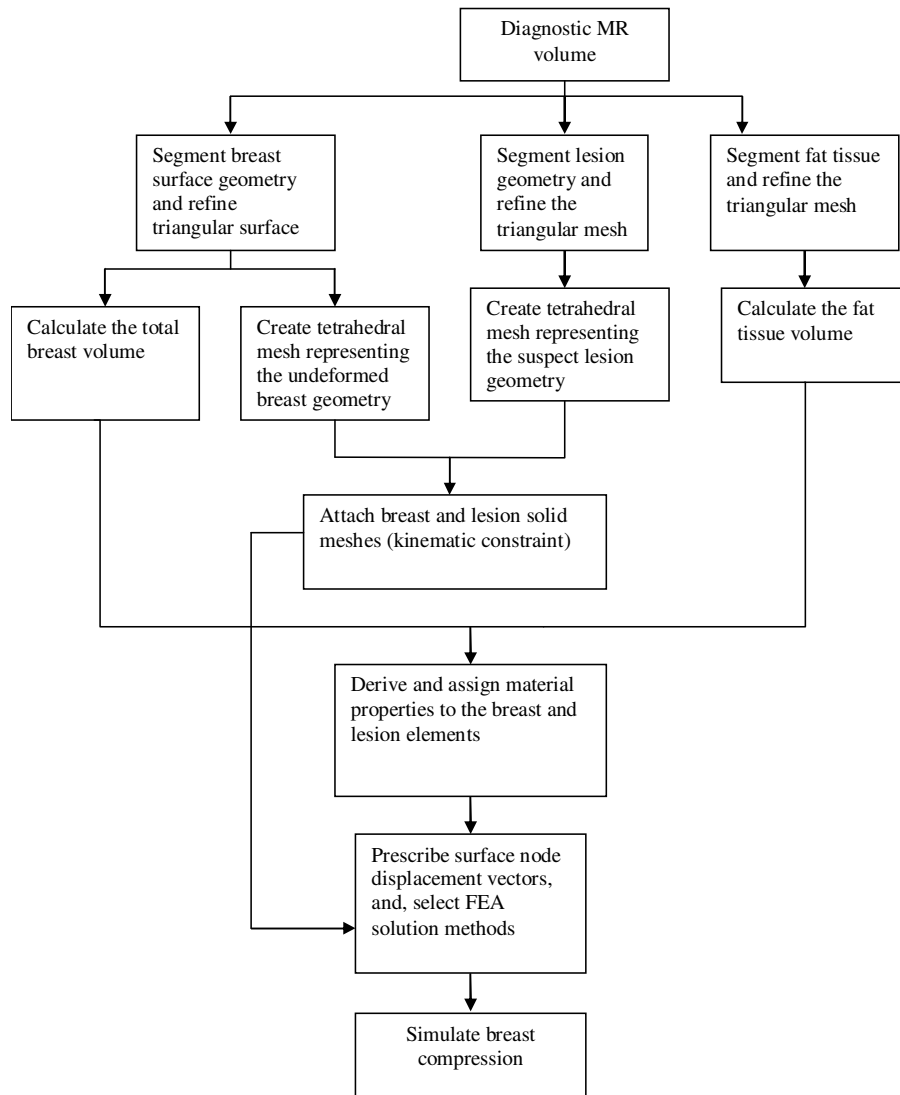


**FIGURE 2:** Overview of the proposed FE breast model construction

### 3.1 MRI Data and Geometry Construction

For this study, the left breast was considered. It contained a single lesion, situated laterally, and was diagnosed as non-invasive cancer. T1-weighted diagnostic and biopsy MR images were acquired. The voxel sizes in the diagnostic and biopsy MR volumes were  $0.94 \times 0.94 \times 2.5 \text{ mm}^3$  and  $0.66 \times 0.66 \times 2 \text{ mm}^3$ , respectively. The biopsy was performed 18 days after the diagnostic MRI exam. Figure 3 contains the 3D rendering of the left breast and a maximum intensity projection (MIP) highlighting the suspect lesion. Figure 4 shows the corresponding biopsy volume.

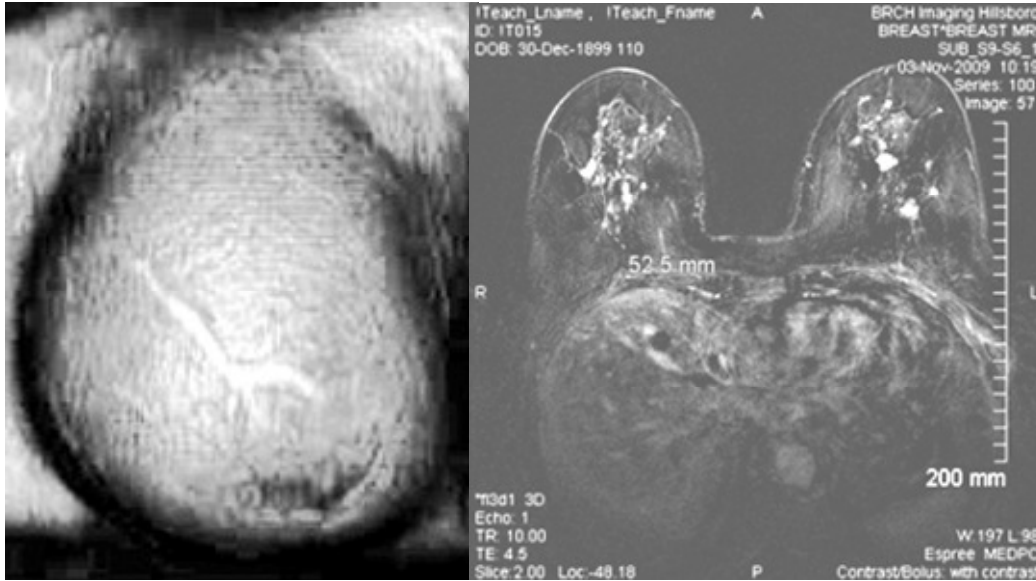


**FIGURE 3:** Breast diagnostic MR volume and a MIP highlighting the suspect lesion

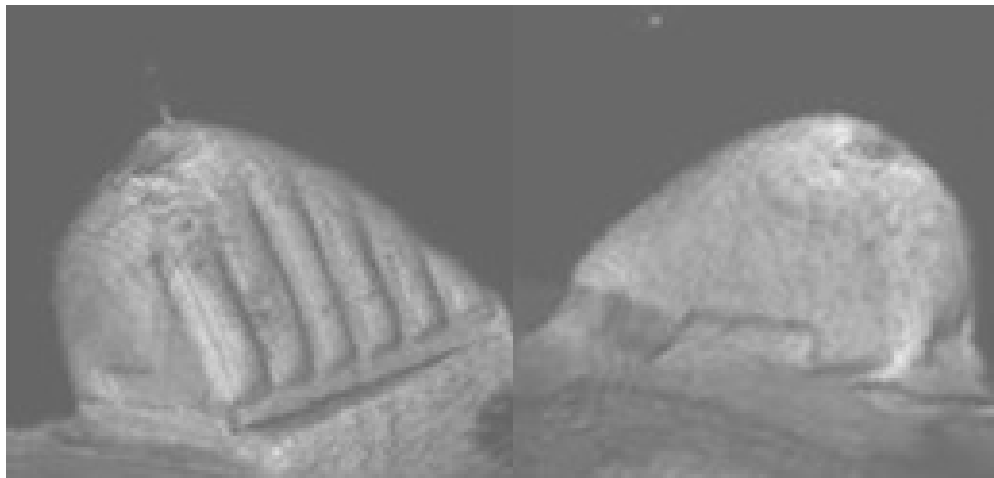


**FIGURE 4:** Breast biopsy MR volume: immobilization plate side (left), compression plate side (right)

### 3.2 MR Volume Rigid Registration

Since the diagnostic and biopsy MR volumes were not aligned, we took an anatomical landmark based registration approach to align these 3D medical images [18]. The sternum was used as the anatomical landmark due to its constant nature [19]. Anatomically, the breast architecture was assumed constant due to scaffolding support by Cooper's ligaments [20]. With sternum alignment, the difference between the two MR volumes was breast compression.

The rigid registration tool in ANALYZE was used to align the two MR volumes, (Fig. 5). This allowed for an independent measurement of lesion displacement (lesion travel from the diagnostic MRI to the biopsy MRI).

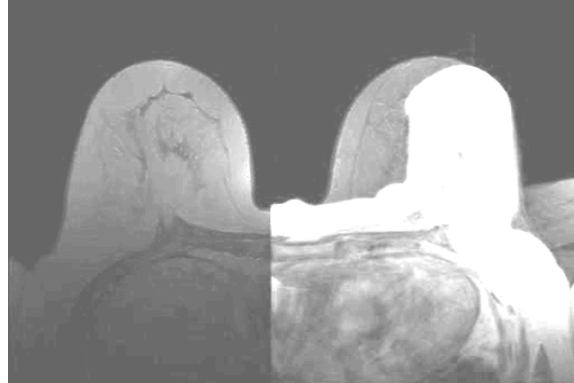


**FIGURE 5:** A 2D MR slice of the biopsy MRI volume (white) overlaid on the diagnostic MR volume (grey), registered at the sternum

### 3.3 Breast and Lesion Geometry Discretization

Figure 6 is a flowchart that describes how the FE breast mesh was constructed; the mesh development process was divided into 5 steps. 1) The diagnostic breast MR images were rendered into a 3D image. 2) Using ANALYZE, we segmented the breast and lesion surfaces from the MR volume. 3) Since the surface mesh quality was insufficient for FEA, these two surfaces were imported into hyperMesh and refined. 4) The breast and lesion surfaces were then independently discretized. The breast surface mesh was discretized resulting in 10,915 tetrahedral elements. The average edge length of the surface elements was 7 mm. The lesion geometry was meshed with a surface element edge length of 0.85 mm resulting in 1,562 tetrahedral elements. 5) We used a kinematic constraint that tied the lesion nodes to the breast nodes based on their isoparametric locations within the breast mesh.

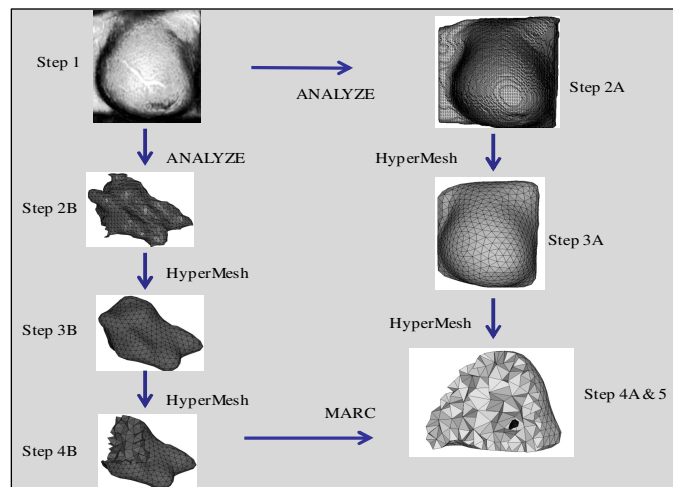


**FIGURE 6:** Breast and lesion geometry discretization process

### 3.4 Elastic Material Properties and Material Model Selection

In this paper, we assumed that the effects of different normal breast tissue types other than the fat and fibroglandular tissues were negligible. In addition, the normal breast tissues were modeled as one tissue type consisting of the volume fractions of the fat and fibroglandular tissues. These volume fractions were calculated by segmenting the fat tissue from the diagnostic MRI and calculating its volume. The total breast volume was also calculated. The fat tissue/total breast volume ratio was 0.67.

Our elastic material properties for the homogeneous breast tissue model were derived by first considering the volume fraction rule,

$$E(\epsilon)_{\text{breast}} = E(\epsilon)_{\text{fat}} V_{\text{fat}} + E(\epsilon)_{\text{fibroglandular}} (1 - V_{\text{fat}}). \quad (8)$$

The variable  $V_{\text{fat}}$  is the volume fraction of fat tissue. The functions  $E(\epsilon)_{\text{fat}}$  and  $E(\epsilon)_{\text{fibroglandular}}$  were derived by fitting Wellman's [7] experimental derived elastic modulus versus strain data for fat and fibroglandular tissues to third order polynomials. Equation (8) was then integrated with respect to strain ( $\epsilon$ ) resulting in the constitutive relationship for the homogeneous breast tissue model, (Fig. 7).

Using Wellman's [7] material property data for lobular cancer, the constitutive relationship for the suspect lesion was similarly derived. The elastic modulus versus strain data was fitted to a third order polynomial and integrated with respect to strain. The corresponding stress versus strain relationship is also shown in (Fig. 7).

The constitutive relationships for the breast and lesion tissues were imported into Mentat and fitted to the Neo-Hookean material model.  $C_{10}$ , the Neo-Hookean material parameter, was 1.1 kPa and 4.2 kPa for the breast and lesion tissues, respectively.

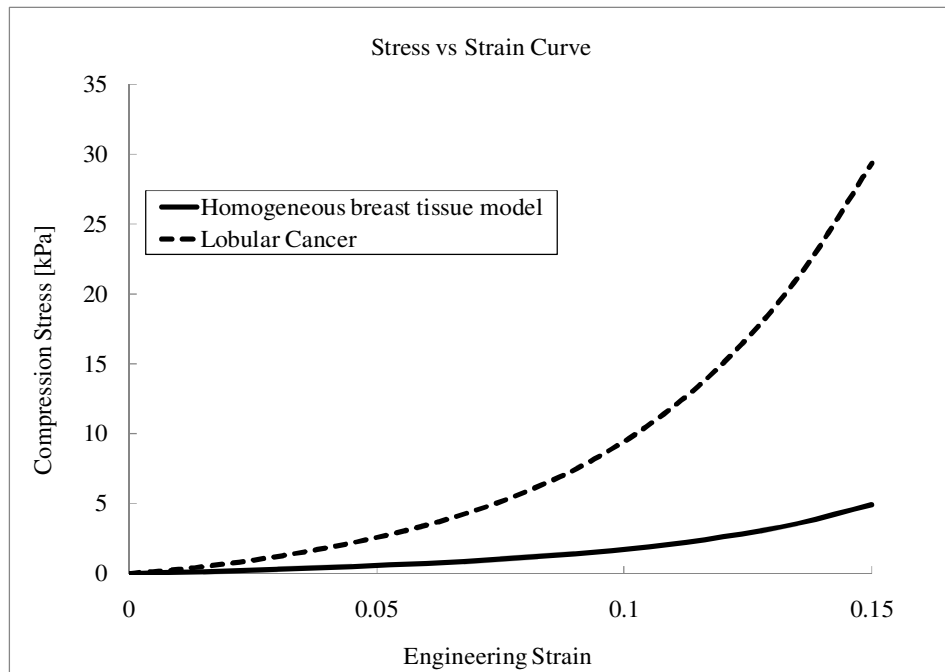
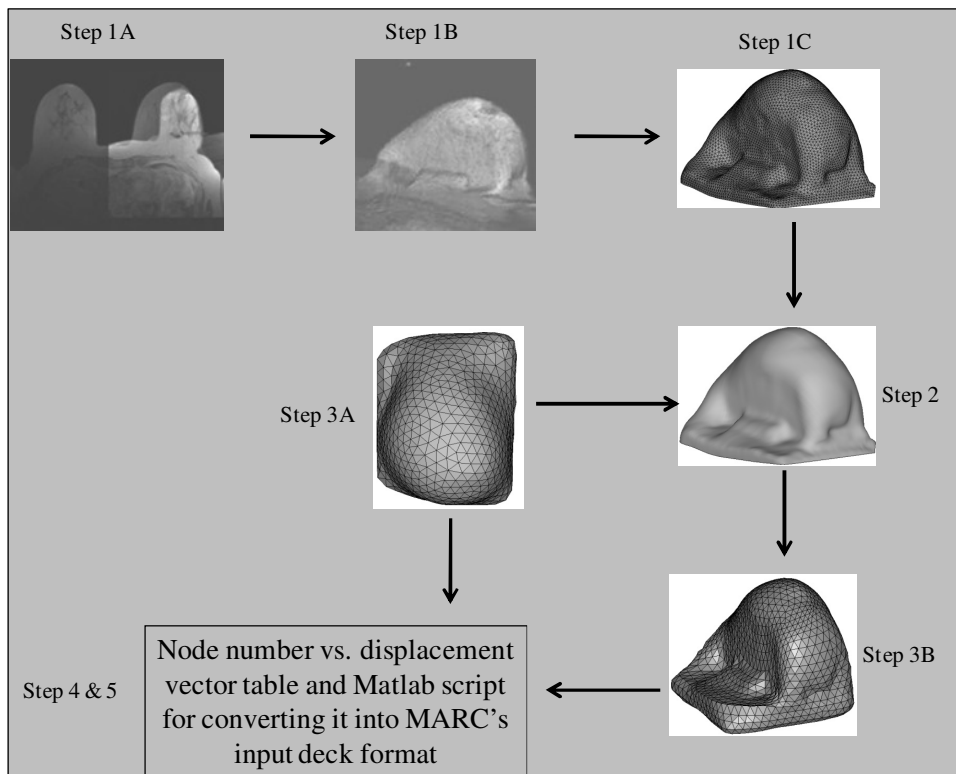


FIGURE 7: Homogenous breast tissue model and lesion stress-strain curves

### Boundary conditions

Fig. 8 is a flowchart that shows how we prescribed a Dirichlet boundary condition, displacement vector, to each surface node. The process that we developed to define the nodal displacement vectors contained 5 steps. 1) With the diagnostic and biopsy MR volumes aligned at the sternum, we segmented the breast surface from the biopsy MR volume. Since the mesh quality was inadequate for FE modeling, it was imported into HyperMesh for refinement. 2) The refined surface mesh was then converted into the Initial Graphics Exchange Specification (IGES) surface format using HyperMesh's mesh to geometry surface modification tool. 3) The uncompressed breast surface mesh, which was used to create the FE breast mesh, was morphed onto the deformed breast IGES surface. 4) From the undeformed and morphed breast surface meshes, the displacement vector for each surface node was calculated by subtracting its position vector on the morphed surface mesh from its position vector on the uncompressed surface mesh.

A node versus displacement vector table was created from these calculations. 5) A script was written that converted the node versus displacement table into MARC input deck format. The output from the script was appended to the input deck of the FE breast model.



**FIGURE 8:** Construction of surface boundary conditions from the biopsy MR

In this study, it was assumed that the nodes at the pectoral fascia and rib interface do not move.

### 3.6 Finite Analysis Solution

Our FEA methodology for simulating breast compression is summarized here:

- **Element Type:** 12,477 linear tetrahedral, full integration Herrmann formulation
- **Contact:** None
- **Links:** insert kinematic constraint (lesion-breast nodes)
- **Boundary Conditions:** displacement controlled
- **Dynamic Effects:** none (quasi static)
- **Solution Control:** large displacement, large strain, Lagrangian, Newton-Raphson
- **Stepping Procedure:** Constant time step
- **Convergence Criteria:** Relative residual force magnitude, criteria  $\leq 0.1$

### 4.0 RESULTS

We constructed 3 additional FE models that differ only in how the suspect lesion was modeled. 1) The lesion was modeled as a rectangular prism made up of 77 tetrahedrals. The suspect lesion was bound by the rectangular prism, similar to the work of Azar et al. [1] 2) A single node representing the centroid of the suspect lesion within the FE breast mesh. Zhang et al. [5] used this method to track a suspect breast feature that was identified on mammographic images. The normal and lesion breast tissue were modeled

as one tissue type consisting of the volume fractions of the fat and fibroglandular tissues. 3) The actual lesion geometry was modeled within the FE breast mesh; a conformal breast-lesion mesh; this method was proposed by Schnabel et al. [3]. The results of these models were compared to the proposed FE model.

The results are arranged into 3 subsections: 1) Deformation contour plots, 2) suspect lesion travel, and 3) suspect lesion overlaid onto the FEA results.

#### 4.1 Deformation Contours Plots

As expected, the displacement contour plots for the four FE lesion models were similar. Figure 9 shows the common displacement contour plot overlaid on the deformed FE breast model after the surface boundary conditions were applied. The deformed surface profile replicates the surface profile of the biopsy MR volume. The peak compression and immobilization plate travel was 46 mm and 15 mm, respectively.

In comparison to the conformal breast-lesion FE mesh, the element count for the proposed FE breast mesh was reduced by 53%, from 26,299 to 12,477 elements. The corresponding time required to apply the surface boundary conditions was reduced from 42 minutes to 3 minutes. The FE model size and processing time differences between models 1, 2, and the proposed FE breast model were negligible.

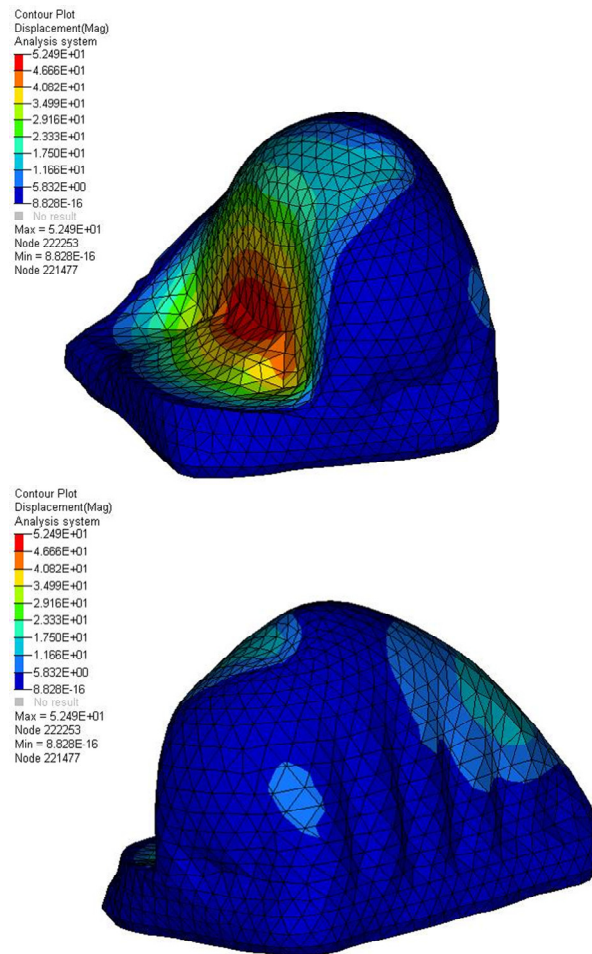


**FIGURE 9:** Displacement contour plots: view from the compression plate side (top) view from the immobilization plate side (bottom)

#### 4.2 Suspect Lesion Travel

ANALYZE was used to calculate the position coordinates of the suspect lesion's centroid in the undeformed and compressed breast volumes. The lesion's displacement vector was calculated by subtracting the lesion's position vector in the biopsy MR volume from the lesion's position vector in the diagnostic MR volume. The centroidal coordinates, in mm, of the lesion from the diagnostic and biopsy MR volumes were (79.7, 219.3, 44.5) and (68.7, 218, 40.1), respectively. From this, the lesion displacement vector was (11, 1.3, 4.3); the corresponding magnitude was 11.9 mm.

Table 1 shows the lesion displacement error from each of the 4 methods used to model the suspect lesion. With 61 mm of breast compression, the proposed FE breast model localized the suspect lesion to within 3.8 mm of its actual position. The accuracy limit for adequate registration is 5 mm [2]. As compared to previously published lesion modeling techniques, the simulation results from the proposed method were provides similar accuracy. Thus, our method for modeling breast lesions may offer the combined benefits of previous researchers without the inherent limitations.

**TABLE 1:** Lesion Centroid Position Error (mm)

	Lesion FE Model	X	Y	Z	Lesion Centroid Position Error
1	Specific Elements within the FE breast Mesh	2.7	1.1	2.3	3.7
2	Single node representing the lesion's centroid within the FE breast Mesh	2.7	1.1	2.4	3.8
3	Actual Lesion geometry within the FE breast Mesh (Confromal breast-lesion mesh)	2.2	1.5	2.3	3.5
4	Actual Lesion geometry within the FE breast Mesh (kinematic constraint)	2.8	1.2	2.3	3.8

#### 4.3 Suspect Lesion Overlaid Onto the FEA Results

Figure 10 shows the actual lesion (right) segmented from the biopsy MR volume, overlaid onto the FEA results (left) from the proposed FE model. The surface areas of the lesion segmented from the diagnostic and biopsy MRI's were 310 mm<sup>2</sup> and 353 mm<sup>2</sup>, respectively. The overlapping surface area was 165 mm<sup>2</sup>. Using the lesion surface area from the diagnostic MR volume, this resulted in 45% overlap. CAD tools were used to calculate the lesion surface areas. The overlapping surface area was created from the intersection of the lesion surfaces.

It is hypothesized that the deviation between these surfaces was due, primarily, to the anisotropic nature of breast tissue [21] and the difference in lesion visualization between the diagnostic and biopsy MR volumes. Breast tissue anisotropy is beyond the scope this paper; modeling anisotropic material behavior may increase the amount of overlap between the actual and predicted lesion positions and should be considered in future research.

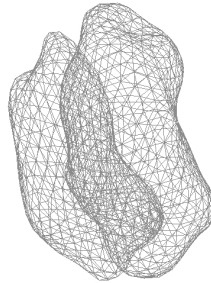


**FIGURE 10:** The actual lesion (left) overlaid onto the FEA results (right). The amount of overlap is highlighted (black)

## 5.0 DISCUSSION

Potentially, radiologists would use our method for modeling suspect lesions, in combination with FEA methods developed by previous researchers, to assist in targeting suspect lesions that are difficult to localize with the breast compressed between rigid plates. Previous researchers have developed stand alone algorithms for segmenting and discretizing the breast surface, lesions, and the fibroglandular tissue region. The physician would simulate breast compression in 3 stages: 1) with the sternum used as a rigid registration feature, they would align the diagnostic and biopsy MR volumes, 2) patient specific suspect lesions would be independently discretized based on their own length scales, and 3) with the lesion meshes kinematically constrained to the corresponding breast mesh, the patient specific FE breast model would then be used to predict the position of the suspect lesion (centroid and boundary positions).

## 6.0 CONCLUSION

In conclusion, this research made three points. 1) The breast and lesion geometries can be independently discretized. A kinematic constraint that tied the lesion nodes to the corresponding nodes in the breast mesh based on their isoparametric position was an enabler for independent breast and lesion meshing. 2) Constructing the surface from the biopsy MR volume and using it to define displacement vectors for the surface of the breast mesh is a viable alternative to prescribing boundary conditions. With this method, the effects of external contacting bodies are considered without having to directly model them. 3) As compared to the conformal breast-lesion mesh, the FE model sized was reduced by 53%.

Since our FEA method was demonstrated on a single case, our evidence is limited to this patient. For this reason, we will use our proposed FEA method to study additional cases. These additional cases will include different types of suspect lesion tissue, lesions situated in different quadrants of the breast, and multiple suspect lesions (dual biopsy).

## 7.0 ACKNOWLEDGEMENTS

The authors would like to thank Dr. Kathy Schilling, Medical Director of Imaging and Intervention for the Boca Radiology Group in Boca Raton, FL. Dr. Schilling supplied the MR image volumes and the corresponding diagnostic detail.

## REFERENCES

- [1] F.S. Azar, D.N. Metaxas, M.D. Schnall. "Methods for modeling and predicting mechanical deformations of the breast under external perturbations". IEEE Workshop on Mathematical Methods in Biomedical Image Analysis, 6(1):1-27, 2002
- [2] N.V. Ruiter, R. Stotzka, T.O. Muller, H. Gemmeke. "Model-based registration of X-ray mammograms and MR images of the female breast". IEEE Symposium Conference on Nuclear Science, 5:3290- 3294, 2004
- [3] A. Schnabel, C. Tanner, A.D. Castellano-Smith, A. Degenhard, M.O. Leach, D.R. Hose, D.L.G. Hill, D.J. Hawkes. "Validation of Nonrigid Image Registration Using Finite-Element Methods: Application to Breast MR Images". IEEE Transactions on Medical Imaging, 22(2):238-247, 2003

- [4] A. Samani, A.J. Bishop, M.J. Yaffe, D.B. Plewes, 2001. "Biomechanical 3-D Finite Element Modeling of the Human Breast Using MRI Data". IEEE Trans. Medical Imag., 20(4):271-279, 2001
- [5] O. Zhang, A. Qiu, D.B. Goldgof, S. Sarkar, L. Li. "3D Finite Element Modeling of Nonrigid Breast Deformation for Feature Registration in X-ray and MR Images". IEEE Workshops on Applications of Computer Vision, :38-44, 2007
- [6] A. Perez del Palomar, B. Calvo, J. Herrero, J. Lopez, M. Doblare. "A Finite Element Model to Accurately Predict Real Deformations of the Breast". Medical Engineering & Physics, 30(9):1089-1097, 2008
- [7] P.S Wellman. "Tactile Sensing". PhD. Thesis, Harvard University, 1999
- [8] T.A Krouskop, T.M. Wheeler, F. Kallel, B.S. Garra, T. Hall. "Elastic Moduli of Breast and Prostate Tissues Under Compression". Ultrasonic Imaging, 20: 260-274, 1998
- [9] J. Bonet, R. Wood. R. "Nonlinear Continuum Mechanics for Finite Element Analysis", Cambridge University Press, pp. 57-64. (1997)
- [10] MSC Software Corporation. "Volume B: Element Library", 2005
- [11] MSC Software Corporation. "Volume A: Theory and User Manual", 2005
- [12] L.R. Herrmann, R.M. Toms. "A reformulation of the Elastic Field Equations in Terms of Displacements, Valid for All Admissible Values of Poisson's Ratio". Journal of Applied Mechanics 31: 148-149, 1964
- [13] R.D. Cook. "Concepts And Applications of Finite Element Analysis 2nd Edition, John Wiley & Sons, pp. 351-353, 1981
- [14] L.R. Herrmann. "Elasticity Equations for Incompressible and Nearly Incompressible Materials by a Variational Theorem". American Institute of Aeronautics and Astronautics (AIAA) 10:1896-1900, 1965
- [15] A.N. Gent. "Engineering with Rubber: How to Design Rubber Components", Hanser Gardner Publications, pp. 50-54, 2001
- [16] AnalyzeDirect. "Analyze 10.0 Essential Training Guide", 2010
- [17] Altair Engineering. "HyperMesh 10.0, User Manual", 2010
- [18] I.N. Bankman. "Handbook of Medical Imaging Processing and Analysis", Academic Press, pp. 499-500, 2000
- [19] M. Betke, H. Hong, D. Thomas, C. Prince, J. Ko. "Landmark Detection in the Chest and Registration of Lung Surfaces with an Application to Nodule Registration". Journal of Medical Image Analysis: 265-281, 2003
- [20] F.H. Netter. "Atlas of Human Anatomy, 2nd ed", Navortis, pp. 167-169, 1997
- [21] C. Tanner, M. White, S. Guarino, S, M.A. Hall-Craggs, M. Douek, M. D.J. Hawkes. "Anisotropic Behavior of Breast Tissue for Large Compressions". IEEE International Symposium on Biomedical Imaging: From Nano to Macro:1223-1226, 2009

## E-Cordial Labeling of Some Mirror Graphs

**S. K. Vaidya**

Department of Mathematics,  
Saurashtra University,  
RAJKOT – 360005, Gujarat (India).

samirkvaidya@yahoo.co.in

**N. B. Vyas**

Department of Mathematics,  
Atmiya Institute of Technology & Science,  
RAJKOT – 360003, Gujarat (India).

niravbvyas@gmail.com

---

### Abstract

Let  $G$  be a bipartite graph with a partite sets  $V_1$  and  $V_2$  and  $G'$  be the copy of  $G$  with corresponding partite sets  $V_1'$  and  $V_2'$ . The mirror graph  $M(G)$  of  $G$  is obtained from  $G$  and  $G'$  by joining each vertex of  $V_1$  to its corresponding vertex in  $V_2$  by an edge. Here we investigate E-cordial labeling of some mirror graphs. We prove that the mirror graphs of even cycle  $C_n$ , even path  $P_n$  and hypercube  $Q_k$  are E-cordial graphs.

**Keywords:** E-Cordial labeling, Edge graceful labeling, Mirror graphs.

---

AMS Subject Classification Number(2010): 05C78

### 1. INTRODUCTION

We begin with finite, connected and undirected graph  $G=(V(G),E(G))$  without loops and multiple edges. For standard terminology and notations we refer to West[1]. The brief summary of definitions and relevant results are given below.

#### Definition 1.1

If the vertices of the graph are assigned values subject to certain condition(s) then it is known as *graph labeling*.

Most of the graph labeling techniques trace their origin to graceful labeling introduced independently by Rosa[3] and Golomb[4] which is defined as follows.

#### Definition 1.2

A function  $f$  is called graceful labeling of graph  $G$  if  $f : V(G) \rightarrow \{0, 1, 2, \dots, q\}$  is injective and the induced function  $f^*(e = uv) = |f(u) - f(v)|$  is bijective. A graph which admits graceful labeling is called a *graceful graph*.

The famous Ringel-Kotzig graceful tree conjecture and illustrious work by Kotzig[5] brought a tide of labeling problems having graceful theme.

#### Definition 1.3

A graph  $G$  is said to be *edge-graceful* if there exists a bijection  $f : E(G) \rightarrow \{1, 2, \dots, |E|\}$  such that the induced mapping  $f^* : V(G) \rightarrow \{0, 1, 2, \dots, |V| - 1\}$  given by  $f^*(x) = \sum_{xy \in E(G)} f(xy) \pmod{|V|}$ ,  $xy \in E(G)$ .

#### Definition 1.4

A mapping  $f : V(G) \rightarrow \{0, 1\}$  is called *binary vertex labeling* of  $G$  and  $f(v)$  is called the *label* of vertex  $v$  of  $G$  under  $f$ .

**Notations 1.5**

For an edge  $e = uv$ , the induced edge labeling  $f^* : E(G) \rightarrow \{0,1\}$  is given by  $f^*(e = uv) = |f(u) - f(v)|$ . Let  $v_f(0), v_f(1)$  be the number of vertices of  $G$  having labels 0 and 1 respectively under  $f$  and let  $e_f(0), e_f(1)$  be the number of edges of  $G$  having labels 0 and 1 respectively under  $f^*$ .

**Definition 1.6**

A binary vertex labeling of graph  $G$  is called a *cordial labeling* if  $|v_f(0) - v_f(1)| \leq 1$  and  $|e_f(0) - e_f(1)| \leq 1$ . A graph  $G$  is called *cordial* if admits cordial labeling.

The concept of cordial labeling was introduced by Cahit[6]. He also investigated several results on this newly introduced concept.

**Definition 1.7**

Let  $G$  be a graph with vertex set  $V(G)$  and edge set  $E(G)$  and let  $f : E(G) \rightarrow \{0,1\}$ . Define on  $V(G)$  by  $f(v) = \sum \{f(uv)^* uv \in E(G)\} \pmod{2}$ . The function  $f$  is called an *E-cordial* labeling of  $G$  if  $|v_f(0) - v_f(1)| \leq 1$  and  $|e_f(0) - e_f(1)| \leq 1$ . A graph is called *E-cordial* if admits *E-cordial* labeling.

In 1997 Yilmaz and Cahit[7] introduced E-cordial labeling as a weaker version of edge-graceful labeling and having flavour of cordial labeling. They proved that the trees with  $n$  vertices,  $K_n, C_n$  are E-cordial if and only if  $n \not\equiv 2 \pmod{4}$  while  $K_{m,n}$  admits E-cordial labeling if and only if  $m + n \not\equiv 2 \pmod{4}$ .

**Definition 1.8**

For a bipartite graph  $G$  with partite sets  $V_1$  and  $V_2$ . Let  $G'$  be the copy of  $G$  and  $V'_1$  and  $V'_2$  be the copies of  $V_1$  and  $V_2$ . The *mirror graph*  $M(G)$  of  $G$  is obtained from  $G$  and  $G'$  by joining each vertex of  $V_2$  to its corresponding vertex in  $V'_2$  by an edge.

Lee and Liu[8] have introduced mirror graph during the discussion of  $k$ -graceful labeling. Devaraj[9] has shown that  $M(m, n)$ , the mirror graph of  $K_{m,n}$  is E-cordial when  $m + n$  is even while the generalized Petersen graph  $P(n, k)$  is E-cordial when  $n$  is even.

In the following section we have investigated some new results on E-cordial labeling for some mirror graphs.

**2. Main Results**

**Theorem 2.1** Mirror graph of even cycle  $C_n$  is E-cordial.

**Proof:** Let  $v_1, v_2, \dots, v_n$  be the vertices and  $e_1, e_2, \dots, e_n$  be the edges of cycle  $C_n$  where  $n$  is even and  $G = C_n$ . Let  $V_1 = \{v_2, v_4, \dots, v_n\}$  and  $V_2 = \{v_1, v_3, \dots, v_{n-1}\}$  be the partite sets of  $C_n$ . Let  $G'$  be the copy of  $G$  and  $V'_1 = \{v'_2, v'_4, \dots, v'_n\}$  and  $V'_2 = \{v'_1, v'_3, \dots, v'_{n-1}\}$  be the copies of  $V_1$  and  $V_2$  respectively. Let  $e'_1, e'_2, \dots, e'_n$  be the edges of  $G'$ . The mirror graph  $M(G)$  of  $G$  is obtained from  $G$  and  $G'$  by joining each vertex of  $V_2$  to its corresponding vertex in  $V'_2$  by additional edges  $e^*_1, e^*_2, \dots, e^*_n$ .

We note that  $|V(M(G))| = 2n$  and  $|E(M(G))| = 2n + \frac{n}{2}$ . Let  $f : E(M(G)) \rightarrow \{0,1\}$  as follows:

For  $1 \leq i \leq n$ :

$$\begin{aligned}
 f(e_i) &= 1; & i \equiv 0, 1 \pmod{4}. \\
 &= 0; & \text{otherwise.} \\
 f(e'_i) &= 1; & i \equiv 1, 2 \pmod{4}. \\
 &= 0; & \text{otherwise.}
 \end{aligned}$$

For  $1 \leq j < \frac{n}{2}$ :

$$\begin{aligned}
 f(e_j^*) &= 1; & j \equiv 1 \pmod{2}. \\
 &= 0; & \text{otherwise.}
 \end{aligned}$$

For  $j = \frac{n}{2}$ :

$$f(e_j^*) = 0.$$

In view of the above defined labeling pattern  $f$  satisfies conditions for E-cordial labeling as shown in Table 1. That is, the mirror graph of even cycle  $C_n$  is E-cordial.

	vertex condition	edge condition
$n \equiv 0 \pmod{4}$	$v_f(0) = v_f(1) = n$	$e_f(0) = e_f(1) = n + \frac{n}{4}$
$n \equiv 2 \pmod{4}$	$v_f(0) = v_f(1) = n$	$e_f(0) + 1 = e_f(1) = n + \left\lceil \frac{n}{4} \right\rceil$

Table 1

**Illustration 2.2:** The E-cordial labeling for the mirror graph of cycle  $C_6$  is shown in Figure 1.

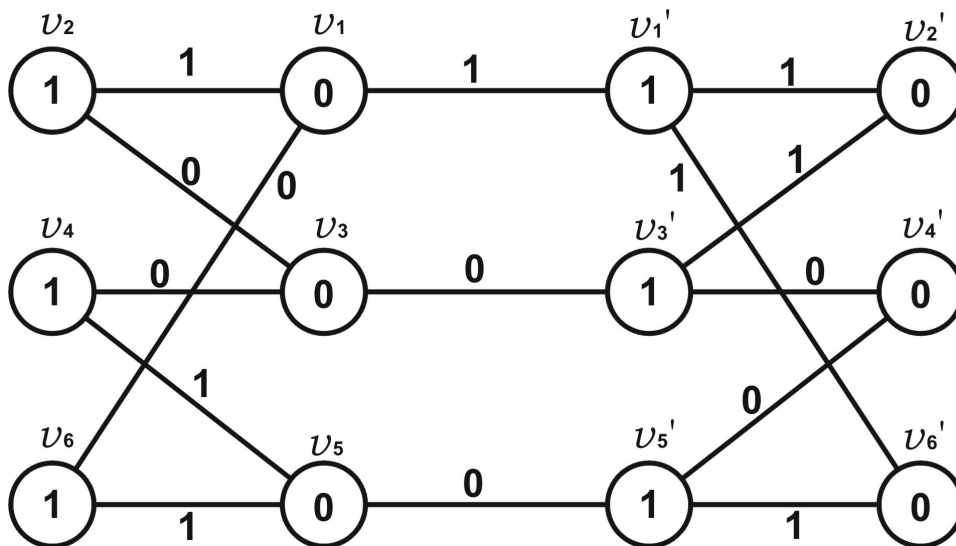


Figure 1

**Theorem 2.3:** Mirror graph of path  $P_n$  is E-cordial for even  $n$ .

**Proof:** Let  $v_1, v_2, \dots, v_n$  be the vertices and  $e_1, e_2, \dots, e_{n-1}$  be the edges of path  $P_n$  where  $n$  is even and  $G = P_n$ .  $P_n$  is a bipartite graph. Let  $V_1 = \{v_2, v_4, \dots, v_n\}$  and  $V_2 = \{v_1, v_3, \dots, v_{n-1}\}$  be the bipartition of  $P_n$ . Let  $G'$  be a copy of  $G$  and  $V'_1 = \{v'_2, v'_4, \dots, v'_n\}$  and  $V'_2 = \{v'_1, v'_3, \dots, v'_{n-1}\}$  be the copies of  $V_1$  and  $V_2$ . Let  $e'_1, e'_2, \dots, e'_{n-1}$  be the edges of  $G'$ . The mirror graph  $M(G)$  of  $G$  is obtained from  $G$  and  $G'$  by

joining each vertex of  $V_2$  to its corresponding vertex in  $V_2'$  by additional edges  $e_1^*, e_2^*, \dots, e_{\frac{n}{2}}^*$ .

We note that  $|V(M(G))| = 2n$  and  $|E(M(G))| = 2(n-1) + \frac{n}{2}$ . Let  $f : E(M(G)) \rightarrow \{0,1\}$  as follows:

For  $1 \leq i < n-1$ :

$$f(e_i) = 1; \quad i \equiv 0, 1 \pmod{4}.$$

$$= 0; \quad \text{otherwise.}$$

For  $i = n-1$ :

$$f(e_i) = 1.$$

For  $1 \leq i \leq n-1$ :

$$f(e'_i) = 1; \quad i \equiv 0, 3 \pmod{4}.$$

$$= 0; \quad \text{otherwise.}$$

For  $1 \leq j \leq \frac{n}{2}$ :

$$f(e_j^*) = 1; \quad j \equiv 0 \pmod{2}.$$

$$= 0; \quad \text{otherwise.}$$

In view of the above defined labeling pattern  $f$  satisfies the conditions for E-cordial labeling as shown in Table 2. That is, the mirror graph of path  $P_n$  is E-cordial for even  $n$ .

	<i>vertex condition</i>	<i>edge condition</i>
$n \equiv 0 \pmod{4}$	$v_f(0) = v_f(1) = n$	$e_f(0) = e_f(1) = n-1 + \frac{n}{4}$
$n \equiv 2 \pmod{4}$	$v_f(0) = v_f(1) = n$	$e_f(0) = e_f(1) + 1 = n-1 + \left\lceil \frac{n}{4} \right\rceil$

Table 2

**Illustration 2.4:** The E-cordial labeling for mirror graph of path  $P_8$  is shown in Figure 2.

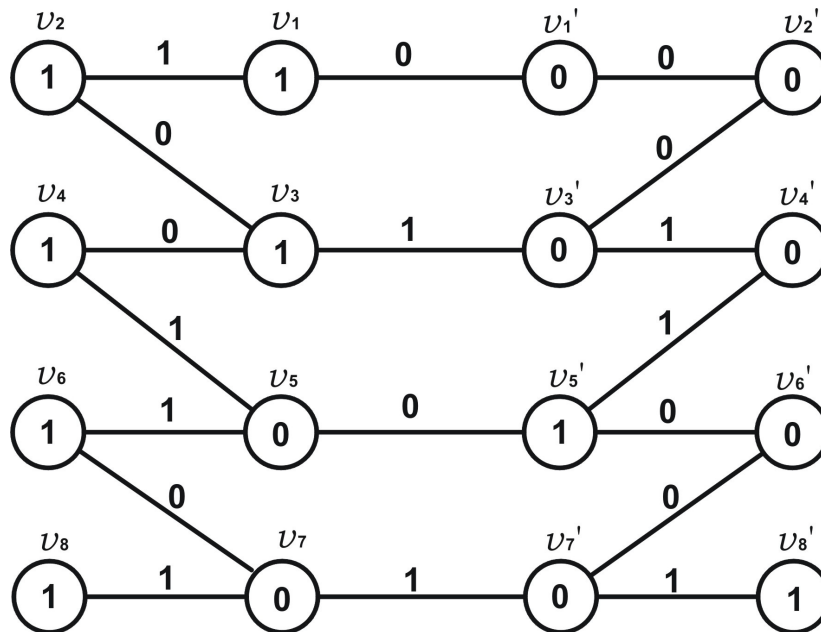


Figure 2.

**Theorem 2.5:** Mirror graph of hypercube  $Q_k$  is E-cordial.

**Proof:**

Let  $G = Q_k$  be a hypercube with  $n$  vertices where  $n = 2^k$ . Let  $V_1$  and  $V_2$  be the bipartition of  $Q_k$  and  $G'$  be a copy of  $G$  with  $V'_1$  and  $V'_2$  be the copies of  $V_1$  and  $V_2$  respectively. Let  $e_1, e_2, \dots, e_m$  be the edges of graph  $G$  and  $e'_1, e'_2, \dots, e'_m$  be the edges of graph  $G'$  where  $m = \frac{nk}{2}$ . The mirror graph  $M(G)$  of  $G$  is obtained from  $G$  and  $G'$  by joining each vertex of  $V_2$  to its corresponding vertex in  $V'_2$  by additional edges  $e_1^*, e_2^*, \dots, e_{\frac{n}{2}}^*$  then  $|V(M(G))| = 2n$  and  $|E(M(G))| = \frac{n(2k+1)}{2}$ .

Define  $f : E(M(G)) \rightarrow \{0,1\}$  as follows:

**Case:1**  $k \equiv 0 \pmod{2}$

Let  $V_i = \{v_{i1}, v_{i2}, \dots, v_{i\frac{n}{2}}\}$  and  $V'_i = \{v'_{i1}, v'_{i2}, \dots, v'_{i\frac{n}{2}}\}$  where  $i = 1, 2$ . All the edges incident to the vertices  $v_{1j}$  and  $v'_{2j}$  where  $j \equiv 1 \pmod{2}$  are assigned the label 0 while the edges incident to the vertices  $v_{1j}$  and  $v'_{2j}$  where  $j \equiv 0 \pmod{2}$  are assigned label 1.

For  $1 \leq j \leq \frac{n}{2}$ :

$$f(e_j^*) = 1; \quad j \equiv 0 \pmod{2}.$$

$$= 0; \quad \text{otherwise.}$$

**Case:2**  $k \equiv 1 \pmod{2}$

For  $1 \leq i \leq n$ :

$$f(e_i) = 1.$$

For  $1 \leq i \leq n$ :

$$f(e'_i) = 0.$$

For  $1 \leq j \leq \frac{n}{2}$ :

$$f(e_j^*) = 1; \quad j \equiv 0 \pmod{2}.$$

$$= 0; \quad \text{otherwise.}$$

In view of the above defined labeling pattern  $f$  satisfies the conditions for E-cordial labeling as shown in Table 3.

	vertex condition	edge condition
$n$	$v_f(0) = v_f(1) = n$	$e_f(0) = e_f(1) = \frac{n(2k+1)}{4}$

**TABLE 3**

That is, the mirror graph of hypercube  $Q_k$  is E-cordial.

**Illustration:2.6**

The E-cordial labeling for mirror graph of hypercube  $Q_3$  is shown in Figure 3.

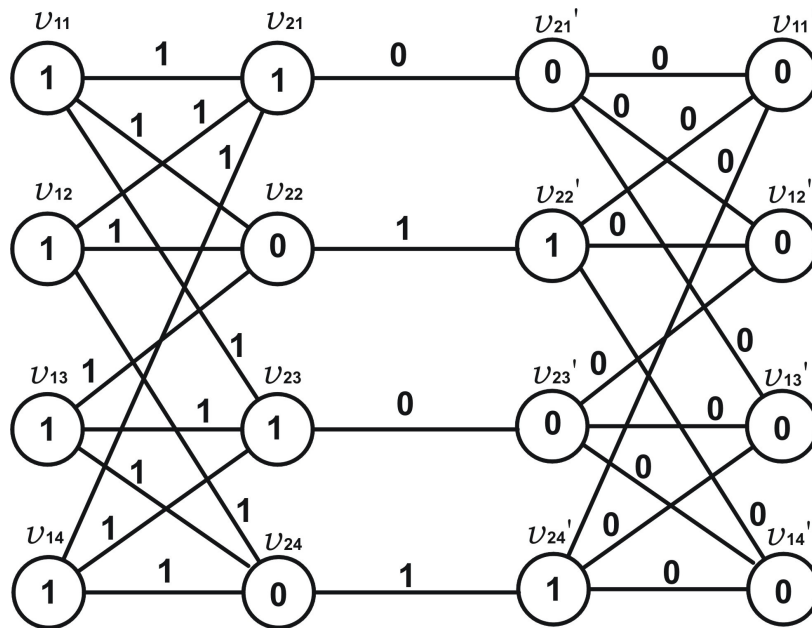


FIGURE 3

### 3. CONCLUDING REMARKS

Here we investigate E-cordial labeling for some mirror graphs. To investigate similar results for other graph families and in the context of different graph labeling problems is an open area of research.

### REFERENCES

- [1] D B West. Introduction To Graph Theory, Prentice-Hall of India, 2001.
- [2] J A Gallian. A dynamic survey of graph labeling, The Electronics Journal of Combinatorics,17, #DS6, 2010. Available: <http://www.combinatorics.org/Surveys/ds6.pdf>
- [3] A. Rosa, On certain valuations of the vertices of a graph, Theory of graphs (Internat. Symposium, Rome, July 1966 ), Gordon and Breach, N. Y. and Dunod Paris (1967), 349-355.
- [4] S. W. Golomb, How to number a graph, in Graph theory and Computing, R. C. Read, ed., Academic Press, New York (1972), 23-37.
- [5] A. Kotzig, On certain vertex valuations of finite graphs, Util. Math., 4(1973), 67-73.
- [6] I Cahit, Cordial Graphs: A weaker version of graceful and harmonious Graphs, Ars Combinatoria, 23(1987), 201-207.
- [7] R. Yilmaz and I. Cahit, E-cordial graphs, Ars. Combin., 46(1997),251-266.
- [8] S. M. Lee and A. Liu, A construction of k-graceful graphs from complete bipartite graphs, SEA Bull. Math., 12(1988), 23-30.
- [9] J. Devaraj, On edge-cordial graphs, Graph Theory Notes of New York, XLVII(2004), 14-18.

## INSTRUCTIONS TO CONTRIBUTORS

The *International Journal of Contemporary Advanced Mathematics (IJCM)* brings together both of these aspects of biology and creates a platform for exploration and progress of these, relatively new disciplines by facilitating the exchange of information in the fields of computing and statistics, mathematics in the Technology sciences are expected to have a substantial impact on the scientific, engineering and economic development of the world. Together they are a comprehensive application of mathematics, statistics, science and computer science with an aim to understand living systems.

We invite specialists, researchers and scientists from the fields of computer science, mathematics, statistics, physics and such related sciences to share their understanding and contributions towards scientific applications that set scientific or policy objectives, motivate method development and demonstrate the operation of new methods in the field of Contemporary Advanced Mathematics.

To build its International reputation, we are disseminating the publication information through Google Books, Google Scholar, Directory of Open Access Journals (DOAJ), Open J Gate, ScientificCommons, Docstoc and many more. Our International Editors are working on establishing ISI listing and a good impact factor for IJCM.

The initial efforts helped to shape the editorial policy and to sharpen the focus of the journal. Starting with volume 2, 2011, IJCM appears in more focused issues. Besides normal publications, IJCM intend to organized special issues on more focused topics. Each special issue will have a designated editor (editors) – either member of the editorial board or another recognized specialist in the respective field.

We are open to contributions, proposals for any topic as well as for editors and reviewers. We understand that it is through the effort of volunteers that CSC Journals continues to grow and flourish.

### LIST OF TOPICS

The realm of International Journal of Contemporary Advanced Mathematics extends, but not limited, to the following:

- Biomedical modelling and computer simulation
- Computational intelligence
- DNA assembly, clustering, and mapping
- Fuzzy logic
- Gene identification and annotation
- Hidden Markov models
- Molecular evolution and phylogeny
- Molecular sequence analysis
- Computational genomics
- Computational proteomics
- E-health
- Gene expression and microarrays
- Genetic algorithms
- High performance computing
- Molecular modelling and simulation
- Neural networks

### CALL FOR PAPERS

---

**Volume: 3 - Issue: 1 - February 2012**

**i. Paper Submission:** November 30, 2011

**ii. Author Notification:** January 01, 2012

**iii. Issue Publication:** January / February 2012

## **CONTACT INFORMATION**

**Computer Science Journals Sdn Bhd**  
B-5-8 Plaza Mont Kiara, Mont Kiara  
50480, Kuala Lumpur, MALAYSIA

Phone: 006 03 6207 1607  
006 03 2782 6991

Fax: 006 03 6207 1697

Email: [cscpress@cscjournals.org](mailto:cscpress@cscjournals.org)

CSC PUBLISHERS © 2011  
COMPUTER SCIENCE JOURNALS SDN BHD  
M-3-19, PLAZA DAMAS  
SRI HARTAMAS  
50480, KUALA LUMPUR  
MALAYSIA

PHONE: 006 03 6207 1607  
006 03 2782 6991

FAX: 006 03 6207 1697  
EMAIL: [cscpress@cscjournals.org](mailto:cscpress@cscjournals.org)